Journal of Catalysis 281 (2011) 345–351

Contents lists available at ScienceDirect

Journal of Catalysis

journal homepage: www.elsevier.com/locate/jcat

An atomic-scale investigation of carbon in MoS_2 hydrotreating catalysts sulfided by organosulfur compounds

Anders Tuxen [a], Henrik Gøbel [a], Berit Hinnemann [b], Zheshen Li [c], Kim G. Knudsen [b], Henrik Topsøe [b], Jeppe V. Lauritsen [a,*], Flemming Besenbacher [a]

[a] Interdisciplinary Nanoscience Center (iNANO) and Department of Physics and Astronomy, Aarhus University, DK-8000 Aarhus C, Denmark
[b] Haldor Topsøe A/S, Nymøllevej 55, DK-2800 Kgs. Lyngby, Denmark
[c] Institute for Storage Ring Facilities, Aarhus University, DK-8000 Aarhus C, Denmark

ARTICLE INFO

Article history:
Received 5 March 2011
Revised 28 April 2011
Accepted 17 May 2011
Available online 25 June 2011

Keywords:
Hydrodesulfurization (HDS)
Scanning Tunneling Microscopy (STM)
Catalysis
Sulfidation
Nanocluster
Sulfur agents
Molybdenum carbide
Coking

ABSTRACT

From an interplay of Scanning Tunneling Microscopy (STM), X-ray Photoelectron Spectroscopy (XPS) experiments, and density functional theory (DFT) calculations, we investigate the fundamental effect of the use of organosulfur compounds for the sulfidation of MoS_2 nanoclusters in the hydrotreating catalyst. Our results reveal that incorporation of carbon in MoS_2-based hydrotreating catalysts as carbide-type phase is not favorable when synthesized with or exposed to dimethyl disulfide (DMDS) or dimethyl sulfide (DMS). These results suggest that substitution of sulfur with carbon on the predominant type of edge structures in MoS_2 nanoclusters is thermodynamically unfavorable, a result that is confirmed by DFT to be valid for all edge structures of MoS_2 exposed under catalytically relevant conditions. However, the results show that the choice of the sulfiding agent can strongly influence the morphology and dispersion of the sulfided phase, and such effects are therefore expected to be of major importance for the activity of the freshly sulfided catalyst.

1. Introduction

The strict limitations regarding the allowed amount of sulfur compounds in fossil fuels have resulted in an increased interest in improving the traditional hydrodesulfurization (HDS) catalyst based on Co and Ni promoted MoS_2. Today, the generally accepted model accounting for the structure of the catalytically active phase in the HDS catalyst is the so-called Co–Mo–S model [1] according to which the catalytically active nanoparticles consist of single- or multilayered MoS_2 structures with the Co or Ni promoter atoms substituting Mo atoms at certain edge sites [2]. Recent STM experiments and density functional theory (DFT) calculations [3–6] have given very detailed insight into the edge structures and how they change upon reaction and synthesis conditions. The edge sites of the Co–Mo–S particles provide the active sites in the HDS reaction, with edge sulfur vacancies acting as the active sites for the direct extrusion of sulfur from S-containing molecules in the oil feed. However, several issues regarding the nature of the active sites in HDS catalysis still remain unresolved. One of the unresolved issues is the possible role of carbon and carbon-containing species. Carbon is known to be a source of catalyst deactivation due to the built-up of coke on the active particles [7], but carbon has also been suggested to have a beneficial effect on the HDS reactivity of MoS_2. For instance, it is recognized in the literature that activation of catalysts with organosulfur agents may result in higher activity than activation with H_2S/H_2 mixtures [8–10]. A beneficial effect of carbon was also reported by Glasson et al. [11], who found that a pre-coked carbon catalyst was more reactive for thiophene conversion than a catalyst not exposed to carbon-containing species. Chianelli and Berhault [12] introduced the idea that in general, elemental carbon can replace sulfur at the MoS_2 edges, giving rise to a carbide-type phase at the edges of the particles. In a recent study by Berhault et al. [13], unsupported MoS_2 particles formed from a $(NH_4)_2MoS_4$ precursor were treated with DMS, and it was suggested that carbon during this treatment replaced edge sulfur atoms leading to a surface carbide phase at the MoS_2 cluster edges. These surface carbide phases were suggested to explain the higher activity of Mo catalysts pre-treated with organosulfur compounds.

The role of carbon in MoS_2-based HDS catalysts has recently been reviewed by Chianelli and co-workers in [14–18]. In these studies, the importance of studying the catalyst in its stabilized state is highlighted, and it is emphasized that carbon substitution is a surface phenomenon occurring only on the surface of

* Corresponding author.
E-mail address: jvang@inano.au.dk (J.V. Lauritsen).

0021-9517/$ - see front matter © 2011 Elsevier Inc. All rights reserved.
doi:10.1016/j.jcat.2011.05.018

the particles. In the present model study, we investigate the basic affinity of carbon to become incorporated into MoS_2 nanoparticles synthesized from a metallic Mo precursor. Our study is focused on the possible incorporation of carbon during the sulfidation with organosulfides. We have used an interplay of Scanning Tunneling Microscopy, X-ray Photoelectron Spectroscopy (XPS), and density functional theory (DFT) calculations to explore the suggested existence of a carbon phase at the edges of MoS_2 nanoclusters. We have characterized the atomic-scale structure of model catalysts composed of MoS_2 nanostructures synthesized by sulfidation of Mo with the two carbon-containing sulfiding agents, DMDS and DMS, and we have investigated the resulting MoS_2 nanoclusters for the possible presence of carbon. DMDS and DMS were chosen because these compounds are commonly used for activation of MoS_2 hydrotreating catalysts. Since chemical bonding of carbon to the MoS_2 particles may occur only at the edges, the concentration of carbon on the surface might be very low. Hence, direct observation of surface carbide phases at MoS_2 nanoclusters is expected to be very challenging. However, Scanning Tunneling Microscopy (STM) is the technique of choice to study our MoS_2 nanoclusters, since STM allows imaging with real space atomic resolution, thus enabling detection of even individual atomic impurities on the clusters. Our STM results reveal that the choice of the sulfiding agent affects the size and shape of the resulting MoS_2 clusters, but the amount of carbon on the MoS_2 particles is extremely low. In fact, for the fully crystalline MoS_2 nanoparticles, we did not observe any carbon at all. XPS spectroscopy reveals some carbon species on poorly crystalline MoS_2 phases, but these do not have a carbide nature and are rather an effect of incomplete sulfidation. Density functional theory (DFT) calculations fully confirm these fundamental STM and XPS findings on the MoS_2 nanocluster catalysts, and the DFT calculations furthermore show that the incorporation of carbon from DMDS and DMS into the MoS_2 structure is thermodynamically unfavorable on all relevant edge structures of MoS_2 exposed under industrial hydrotreating conditions.

2. Experimental and computational details

2.1. Scanning Tunneling Microscopy (STM)

The STM experiments were carried out in a standard UHV chamber with a base pressure below 1×10^{-10} mbar. The chamber is equipped with the Aarhus STM described in Ref. [19], and is capable of achieving atomic resolution on a routine basis. As model support, we use the Au(1 1 1) substrate used in our previous studies [20–22] to address the atomic-scale structure of MoS_2 and Co–Mo–S nanoclusters as this substrate allows us to image the detailed atomic structure of the edges with STM microscopy and to use element specific XPS spectroscopy. In this study, we shed light on the role of the particular compounds used for the sulfidation of Mo into MoS_2 using three sulfidation agents for the synthesis of MoS_2 nanoclusters on the Au substrate, hydrogen sulfide gas (H_2S, Praxair 99.8%), dimethyl disulfide (DMDS, CH_3–S–S–CH_3, Sigma Aldrich 98%), and dimethyl sulfide (DMS, CH_3–S–CH_3, Sigma Aldrich 99%). The synthesis begins with dosing of the sulfur agent to the clean Au(1 1 1) sample at a pressure of 1×10^{-7} mbar. The pressure of hydrogen during the synthesis was measured with a quadrupole mass spectrometer to be 5×10^{-10} mbar. Subsequently, Mo is deposited from an Oxford e-beam evaporator onto the sample, and the deposition of Mo in the sulfur agent continues until a coverage corresponding to approximately 10% of a monolayer is achieved. Finally, the sample is postannealed for 10 min to 673 K or 723 K while the flux of the sulfidation agent to the sample is maintained. Numerous STM studies have shown that this synthesis procedure leads to mainly single-layered MoS_2 nanoclusters with a size ranging from 1 to 3 nm [20,22,23].

2.2. X-ray Photoelectron Spectroscopy (XPS)

XPS measurements were performed on the SX700 beamline at the ASTRID synchrotron, at Aarhus University. All measurements were performed with a fixed 100 mm mean radius analyzer (VG-CLAM2) and with the sample in normal emission with respect to the detector. The typical resolution is 0.5 eV for this setup. MoS_2 nanoclusters were synthesized on the same Au(1 1 1) sample used for the STM experiments and following the exact same synthesis parameters as in the STM experiments to ensure the same synthesis conditions. MoS_2 nanostructures are easily oxidized, and in order to avoid oxidation effects that may occur if pre-synthesized samples are transferred to the UHV chamber for measurements, we have chosen to synthesize the MoS_2 nanoclusters samples directly in the UHV chamber at the beamline. The MoS_2 coverage on the Au(1 1 1) surface in the XPS experiments was calibrated by transferring the sample to the STM chamber. The XPS data were fitted using a parabola background and the FitXPS 2.12 program [24].

2.3. Density functional theory (DFT)

The density functional theory (DFT) calculations were carried out for an infinite stripe model of MoS_2 analogous to Refs. [4,22,25,26], which exposes the $(1\,0\,\bar{1}\,0)$ Mo-edge on one side and the $(\bar{1}\,0\,1\,0)$ S-edge on the other side. We use a stripe containing two Mo atoms in the x direction and four Mo atoms in the y direction, denoted as a 2×4 model. The stripes are separated by 14.8 Å in the z direction and 9 Å in the y direction. It is known from previous studies that under the sulfur-rich conditions in the STM experiment, the Mo-edge with dimers (100% S coverage) is exposed, whereas under hydrotreating conditions the Mo-edge is terminated by sulfur monomers (50% S coverage) and adsorbed hydrogen [4,22,27]. Under sulfur-rich conditions, the S-edge is not exposed at all, whereas under hydrotreating conditions it is terminated by sulfur dimers and adsorbed hydrogen [4,22]. As the hydrogen coverage on the Mo-edge is between 0.25 and 0.5 under hydrotreating conditions [27,28], we consider the Mo-edge both with 0.5 coverage of adsorbed hydrogen and without adsorbed hydrogen. The relevant edge structures are depicted in Table 1.

DACAPO [29,30], a plane wave density functional theory code, is used in the DFT calculations. The Brillouin zone is sampled by a Monkhorst–Pack $4 \times 1 \times 1$ k-point set [31] with four k-points in the x direction and gamma-point sampling in the other directions. We use a 30 Rydberg plane wave cutoff and 45 Rydberg density wave cutoff [32]. Ultrasoft pseudopotentials [33] are used except for sulfur, for which a soft pseudopotential is used [34]. The Fermi temperature is chosen to be 0.1 eV, and all energies are extrapolated to zero electronic temperature. As exchange–correlation functional, we use the revised Perdew–Burke–Ernzerhoff (RPBE) functional [29]. We calculate a MoS_2 equilibrium lattice parameter of 3.24 Å, which is in good agreement with the experimental lattice parameter of 3.16 Å [35]. We relax all structures, until all force components of all atoms are below 0.02 eV/Å. We also tested tighter force convergence criteria, but found only negligible differences in resulting structures and energies.

We calculate the energy for carbon substitution ΔE_{Csub} as follows

$$\Delta E_{\mathrm{Csub}} = E(\mathrm{Mo}_x\mathrm{S}_{y-1}\mathrm{CH}_{z+a}) + E_{\mathrm{S}} - [E(\mathrm{Mo}_x\mathrm{S}_y\mathrm{H}_z) + E_{\mathrm{C}} + aE_{\mathrm{H}}] \qquad (1)$$

In this equation, we assume that one sulfur atom is replaced by a CH_a fragment. As all sulfur atoms in the MoS_2 edge structures have at least two bonds to either neighboring Mo or S atoms, we

Table 1
Employed DFT model for MoS_2 structure and relevant edge terminations under both STM and hydrotreating conditions.

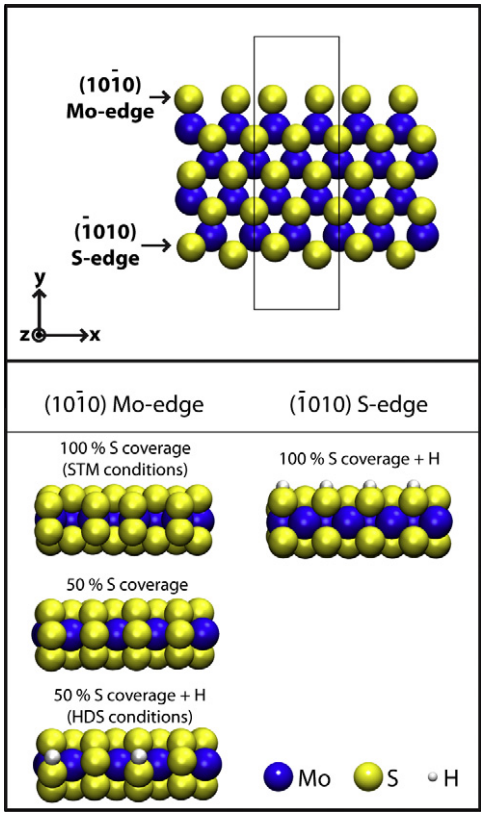

consider substitution of C, CH, and CH_2 for S. $E(Mo_xS_{y-1}CH_{z+a})$ is the DFT energy of the structure, in which one S is substituted by CH_a, and $E(Mo_xS_yH_z)$ is the energy of the structure before substitution. E_S, E_H, and E_C are the reference energies for sulfur, hydrogen, and carbon, respectively.

With respect to the choice of reference energies for sulfur, we refer the energy to the deposition of sulfur from H_2S with concurrent production of one H_2 molecule

$$\Delta E_S = E(H_2S) - E(H_2) \quad (2)$$

In this equation, $E(H_2S)$ is the energy of one H_2S molecule in the gas phase and $E(H_2)$ is the energy of one H_2 molecule in the gas phase. This sulfur reference has been used previously to calculate phase diagrams of edge structures under different conditions [4]. Likewise, we reference hydrogen to H_2 in the gas phase

$$\Delta E_H = \frac{1}{2}E(H_2) \quad (3)$$

We reference the carbon energy to both the DMDS and the DMS molecules, as these two molecules are used for sulfidization. The carbon reference energy for DMDS $E_{C,DMDS}$ is given by

$$\Delta E_{C,DMDS} = \frac{1}{2}E(DMDS) - E_S - 3E_H \quad (4)$$

with E(DMDS) as the DFT energy of the DMDS molecule in the gas phase. The carbon reference energy for DMS $E_{C,DMS}$ is given by

$$\Delta E_{C,DMS} = \frac{1}{2}E(DMS) - \frac{1}{2}E_S - 3E_H \quad (5)$$

Table 2
Carbon reference energies of different carbon sources referenced to graphene. For translation of results obtained with one carbon reference to another one, the difference of the two reference energies needs to be subtracted.

Molecule	$E_{C,molecule} - E_{C,graphene}$ (eV)
Methane, CH_4	−1.23
DMS, CH_3–S–CH_3	−0.42
DMDS, CH_3–S–S–CH_3	−0.22
Benzene, C_6H_6	−0.07
Graphene	0
Carbon disulfide, CS_2	1.30
CH	6.05
Atomic carbon, C	7.35

It should be noted that in a previous theoretical study of carbon incorporation into MoS_2 [36], different choices for the carbon references were chosen, and instead, carbon was referenced to an atomic carbon atom and to a CH fragment. To aid comparison of results obtained using different carbon references, we calculate carbon energies from different molecules and reference them to graphene (we choose graphene instead of graphite because of the well-known problems of DFT with van der Waals forces). The calculated energies are shown in Table 2.

Table 2 demonstrates that the carbon substitution energies will depend on the carbon source, since atomic carbon atoms are of course much more reactive and higher in energy than for instance carbon supplied by organosulfides or hydrocarbons.

It should also be noted that in Ref. [36] sulfur was referenced to a sulfur atom and not to H_2S and H_2, as we do here. We calculate that the sulfur atom reference is lying 3.34 eV higher than the E_S from Eq. (2).

3. Results and discussion

To investigate the possible incorporation of carbon in MoS_2 nanoclusters, we synthesized MoS_2 nanoclusters with two different carbon-containing sulfur agents, dimethyl disulfide (DMDS) and dimethyl sulfide (DMS), and compared them to nanoclusters synthesized with the pure H_2S sulfiding agent. In Fig. 1, we first show large-scale STM images revealing the morphology of MoS_2 clusters synthesized with H_2S and DMDS at 673 K. The morphology of the synthesized structures is directly comparable, since they are prepared with exactly the same preparation procedure (see Section 2), and hence, the only parameter varied between the two experiments is the type of sulfur agent. In both cases, a distinct triangular morphology is revealed from the STM images of the MoS_2 nanoclusters. The average STM height of the nanoparticles is in both cases measured to be 2.3 Å, which is close to the geometric height of 3.16 Å for single-layered MoS_2 nanoclusters oriented with the (0 0 0 1) basal plane in parallel with the substrate [20]. The slight underestimation of the cluster height by STM is attributed to (i) electronic effects resulting from the semiconducting character of the MoS_2 nanoparticles and (ii) the fact that STM images record the local density of states at the Fermi level projected to the apex position of the tip above the surface, and thus the STM images reflect both the geometrical and electronic structure of the semiconducting MoS_2 clusters.

The atomic-scale structure of the MoS_2 clusters synthesized with H_2S in Fig. 1a has been described in detail previously [22,23]. The triangular clusters consist of crystalline MoS_2, which preferentially expose the (10$\bar{1}$0) Mo-edge termination of MoS_2. Under these sulfiding conditions, the edges of the clusters are terminated by sulfur (S_2) dimers and thus fully saturated with sulfur. An important characteristic of the clusters is the brim states revealed in the STM images at the perimeter of the cluster and more

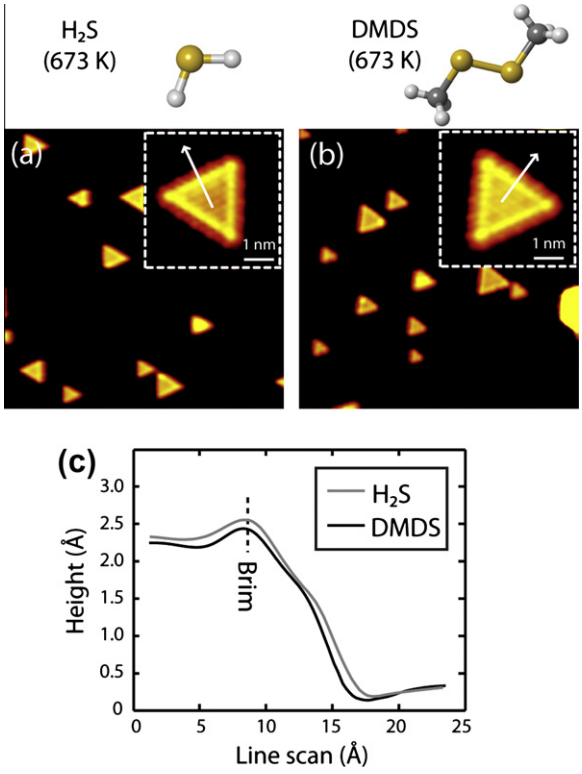

Fig. 1. STM images (300 × 300 Å^2) of MoS_2 nanoclusters synthesized with (a) H_2S and (b) DMDS at 673 K. The inset images show close-up images of the synthesized nanoclusters. (c) Line scans perpendicular to the edges of clusters in the inset images in (a) and (b).

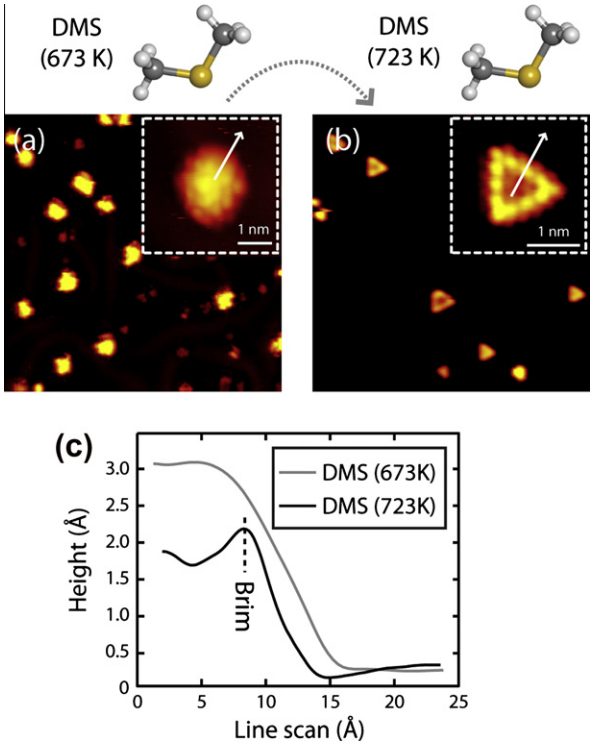

Fig. 2. STM images (300 × 300 Å^2) of MoS_2 nanoclusters synthesized with (a) DMS at 673 K and (b) DMS at 723 K. The inset images show close-up images of the synthesized nanoclusters. (c) Line scans perpendicular to the edges of clusters in the inset images in (a) and (b).

clearly revealed on the inset image in Fig. 1a. The brim originates from a metallic electronic state located at the edge of the MoS_2 nanoclusters, and as such, these edge states are very sensitive to local changes in the composition and morphology of the MoS_2 nanoclusters [25]. In Fig. 1c, we display line scans recorded perpendicular to the edges of the particles over the brim. If carbon incorporation has taken place, this would lead to significant structural and electronic changes at the edges, which should be easily detectable in the line scans. However, the line scans reveal that the STM height profile over the edges is quantitatively and qualitatively indistinguishable for the clusters, reflecting identical Mo-edge terminated structures and identical S coverage of 100%, irrespective of the sulfidation agent. The STM image in Fig. 1b furthermore reveals that the MoS_2 clusters synthesized with the carbon-containing DMDS agent have the same detailed structure and distinct triangular morphology as observed with H_2S. The high-resolution image in Fig. 1b further reveals that the atomic structure of the clusters synthesized with DMDS is similar to the clusters synthesized with H_2S. This further supports that no carbon is incorporated at the surface or the interior of the particles when DMDS is used instead of H_2S.

The STM image in Fig. 2a reveals that the clusters synthesized with DMS at 673 K are indeed very different from those synthesized with H_2S or DMDS under the same conditions. Firstly, the clusters do no longer exhibit the distinct triangular shape, which was observed with H_2S or DMDS. Instead, the clusters appear to have an amorphous morphology, and the detailed atomic structure of the nanoclusters could no longer be resolved with STM. Another important difference is reflected in the line scans in Fig. 2c, which show that the maximum STM height of the cluster is approximately 3.0 Å, and thus significantly higher than the typical value of 2.3 Å observed for the single-layered MoS_2 nanoclusters synthesized with DMDS or H_2S. However, when the clusters are annealed to a slightly higher temperature of 723 K (Fig. 2b), the observed

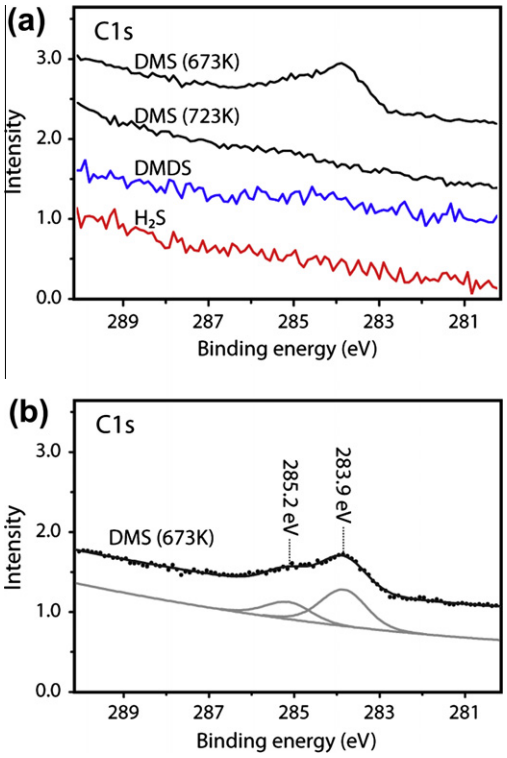

Fig. 3. (a) XPS spectra of the C1s peaks of MoS_2 clusters (photon energy = 375 eV). (b) Fitting of the C1s peak for the clusters synthesized with DMS at 673 K.

morphology changes significantly into the distinct triangular shape, characteristic for the formation of crystalline MoS_2 nanoclusters. The high-resolution STM in the insert image in Fig. 2b and the line scan in Fig. 2c also clearly reveal the brim state at the edges of the nanoclusters, further supporting that the MoS_2 nanoclusters have now obtained a crystalline MoS_2 structure.

We have used XPS to determine the chemical composition of the nanoclusters. In Fig. 3a, we show the energy region of the C1s peak after the synthesis with the three agents DMDS, DMS, and H_2S. The C1s spectra clearly reveal no carbon peak after H_2S and DMDS sulfidation, which strongly corroborates the conclusion from the STM results that carbon is not present in the interior or at the surface of the nanoclusters when they are synthesized with these two sulfiding agents. However, for the clusters synthesized with DMS at 673 K, we observe a small C1s peak. Using sensitivity factors for the respective photon energies for the Mo3d and C1s peaks, we find a C/Mo ratio of 0.18 for this sample. However, the carbon peaks completely disappear upon annealing to 723 K. Comparing this result with the STM results presented in Fig. 2a and b, it is concluded that the amorphous structure observed in the STM image in Fig. 2a must include residual carbon for example in the form of thiolate species [37], which upon annealing to 723 K desorbs from the surface of the clusters as they obtain a crystalline structure. XPS spectra of the Mo3d and S2p peaks (not shown here) reveal that the nanoclusters consist only of Mo and S with binding energies consistent with those reported previously for crystalline MoS_2 nanoclusters on Au(1 1 1) [38].

The shape of the carbon 1s peak observed for clusters synthesized with DMS at 673 K is rather broad, which indicates that more than one type of carbon exists on the surface of the MoS_2 clusters. The C1s peak is fitted with two components corresponding to two different types of carbon on the surface (Fig. 3b). The first component is located at a binding energy of 285.2 eV, which is close to the energy expected for carbon binding to sulfur [39,40]. We thus assign this peak to carbon stemming from the incomplete decomposition of DMS. The second component is located at a slightly lower binding energy of 283.9 eV. We assign this peak to carbon interacting with Mo, but the binding energy of this component is too high to be carbon in a carbide phase for which a binding energy of 283.3 eV is expected [41]. Moreover, both of these two components disappear in the XPS spectra upon annealing slightly higher to 723 K, indicating that the carbon-containing species have desorbed. These results show that even though we start out by having carbon in close proximity to the molybdenum atoms, the carbon atoms have no apparent tendency to bind strongly to Mo in the final sulfided MoS_2 phase. Instead, the minor C components in the incomplete sulfided samples are considered to arise from residue carbon from incomplete sulfidation and crystallization of the nanoclusters when using DMS. The carbon residues observed with DMS at 673 K could be due to DMS being only partly decomposed as observed in [42] since this would explain why carbon is observed on the particles. The lack of carbon after sulfidation with DMDS could on the other hand be due DMDS decomposing to DMS and H_2S as described in [43] in the presence of hydrogen or a direct extraction of sulfur from DMDS with the formation of DMS in the absence of hydrogen.

We have used DFT calculation to explore in further detail the thermodynamics of carbon incorporation into MoS_2, by calculating various carbon configurations in MoS_2 nanoclusters. We start out by considering the fully sulfided Mo-edge terminated by sulfur dimers (the structure present in the STM samples) and investigate carbon substitution for an edge sulfur atom (see Table 3), a sulfur atom in the second row and an edge molybdenum atom (in the latter case, we take the molybdenum reference from MoS_2 as reference). We find that the substitution of a sulfur atom in the second row is 1.36 eV more unfavorable than the substitution of edge sulfur, and substitution of molybdenum is even more unfavorable with 2.17 eV. We, therefore, conclude that edge sulfur atoms are the most likely candidates for carbon substitution and concentrate on these sites in the following.

For the edge sulfur atoms on the Mo-edge, we present in Table 3 the results for carbon substitution on edges with both the sulfur dimer termination (Mo1–Mo3), which are present under the sulfur-rich STM conditions, and the sulfur monomer termination with (Mo7–Mo9) and without hydrogen (Mo4–Mo6). The latter structures are expected to dominate under real industrial HDS conditions. To investigate the stability of different carbon species, we substitute not only with C but also with CH and CH_2. The overall trend for the substitution energies shown in Table 3 is that all energies are endothermic for both DMS and DMDS as carbon references. Thus, it is thermodynamically unfavorable to substitute edge sulfur by either C, CH, or CH_2 if the carbon is supplied by DMS or DMDS. The calculations in Table 3 reveal some interesting trends for the substitution of sulfur with carbon. The lowest forma-

Table 3
DFT calculations on C, CH, and CH_2 substitutions of S atoms at the $(10\bar{1}0)$ Mo-edge, both under STM conditions with sulfur dimers and under HDS conditions with sulfur monomers. Here, we consider the edge both with and without adsorbed hydrogen. For the Mo-edge with sulfur monomers and 50%, only substitution of S atoms is investigated, since substitution of SH atoms leads to the same structures as for the Mo-edge with sulfur monomers.

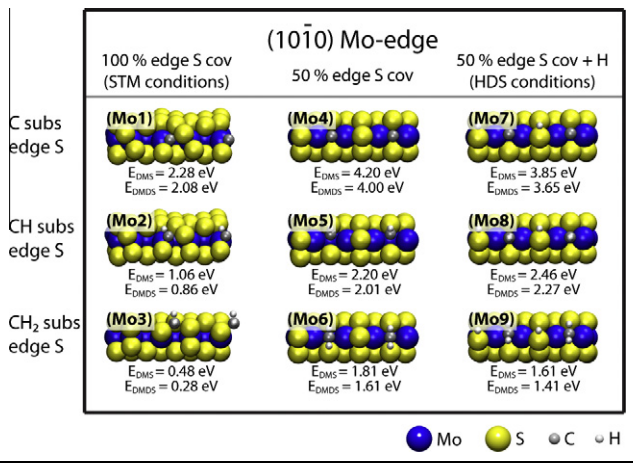

Table 4
DFT calculations on C, CH, and CH_2 substitutions of S atoms at the $(\bar{1}010)$ S-edge. The S-edge is terminated by sulfur dimers and adsorbed hydrogen. Both substitution of S and SH have been considered.

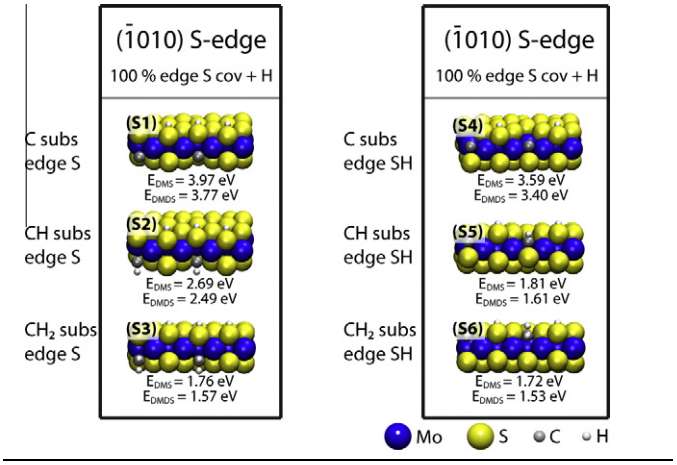

tion energies are found on the Mo-edge with 100% coverage of sulfur; hence, it would appear that a higher coverage of sulfur makes the substitution less endothermic. This result is to be expected as the sulfur dimers are more weakly bound to the edge than the sulfur monomers, and therefore, it is less endothermic to substitute one sulfur atom in a dimer with carbon than in a monomer. This implies that the substitution of sulfur with carbon is even more unfavorable under HDS operating conditions where the edges contain less sulfur than under the sulfur-rich conditions used in the STM and XPS experiments on the MoS_2 model catalysts. The lowest substitution energy for carbon on the Mo-edge is obtained when a sulfur atom on the 100% edge is substituted with a CH_2 group. This substitution is still endothermic with 0.28 eV.

In Table 4, we also consider carbon substitution of edge sulfur for the S-edge, which under both STM and HDS conditions has a full coverage of sulfur with adsorbed hydrogen on the edges. Substitution of S as well as S–H groups at the edges is investigated, since hydrogen generally binds strongly to the S-edge. The general conclusion for the S-edge is the same as for the Mo-edge, and all investigated carbon substitution structures are energetically unfavorable, i.e., endothermic if carbon is supplied by DMS or DMDS. The substitution energies are seen to depend on whether sulfur or SH is substituted, with carbon substitution with SH being slightly less unfavorable than substitution with S. Nonetheless, the overall conclusion is that carbon substitution is endothermic in all investigated cases. It should also be remarked that carbon substitution with methane as carbon reference (see Table 2) is even more endothermic, as the methane reference lies below the DMDS and DMS references. Therefore, carbon incorporated into the MoS_2 structure would not be stable during operation toward replacement by sulfur and desorption as CH_4.

When investigating the substitution energies for the Mo-edge and the S-edge in Tables 3 and 4, it appears that there is a quite general trend for sulfur substitution with C, CH, and CH_2. Substitution with CH_2 is always less unfavorable than with C while an intermediate energy is obtained with CH. This trend is highlighted in the plot in Fig. 4 where we plot the substitution energies in Tables 3 and 4 as a function of the carbon species C, CH, and CH_2. It is evident from Fig. 4 that all edges have quite similar substitution energies for C, CH, and CH_2 (around 4 eV for C, 2–3 eV for CH with a larger variation and 2 eV for CH_2) except for the 100% sulfur terminated Mo-edge for which the substitution energies are significantly lower. This can be rationalized as follows: the coordination environment of the substituted sulfur atom is similar for the 50% sulfur terminated Mo-edge and the 100% sulfur terminated S-edge, as sulfur here is coordinated in a bridge position to two Mo atoms. In contrast, on the 100% sulfur terminated Mo-edge, sulfur interacts primarily with the other sulfur atom in the dimer and with one Mo atom. This coordination environment is different, leading to lower substitution energies. The presence of hydrogen also accounts for some of the variation in substitution energies, as substitution of SH leads to slightly different energetics compared with substitution of S.

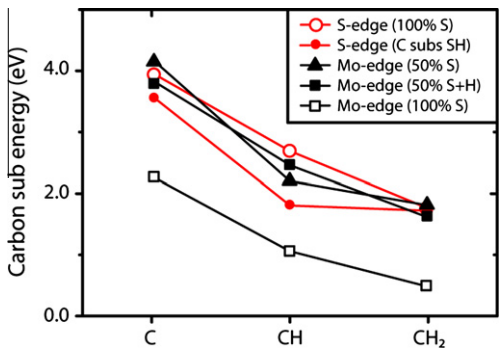

Fig. 4. Plot of DFT formation energies for carbon substitution with C, CH, and CH_2. DMS is used as carbon reference.

The second trend visible in Fig. 4 is that the substitution energies decrease from C to CH to CH_2. This is not surprising, since in a simple picture of bond order conservation one would expect the weakening of the bond strength of CH_x to the Mo atoms to be proportional to the number x of H atoms in the CH_x fragment. This would lead to an ordering of the substitution energies C > CH > CH_2 which is what our DFT results show. These considerations stem from the extensive scaling relationships for CH_x, NH_x, OH_x, and SH_x molecules recently developed both for transition metal surfaces [44] and for oxide, nitride, and sulfide surfaces [45]. The latter study includes all sulfides existing in the MoS_2 crystal structure. In particular, it was found for the metal surfaces that the more H atoms added in the CH_x fragment, the weaker the binding to the surface [44]. For sulfides, it was likewise demonstrated [45] that SH binds weaker than S. Here, we thus demonstrate the same effect for CH_x fragments on the edges of MoS_2.

It is interesting to compare our results to a previous study by Wen et al. [36], who investigated sulfur substitution by carbon in MoS_2 clusters by DFT calculations. They found that sulfur substitution by carbon is strongly exothermic when atomic carbon and CH fragments were used as references for carbon and atomic sulfur as sulfur reference. By means of Table 1, we can translate their results with atomic C and S as references to e.g., our E_S from H_2S and H_2 and E_C from DMS. If we e.g., translate their energy of −0.77 eV for substitution of sulfur by carbon for the Mo-edge terminated by sulfur monomers (referenced to atomic sulfur and carbon), this corresponds to an energy of 3.46 eV (referenced to E_S from Eq. (2) and $E_{C,DMS}$ from Eq. (5)). For the same substitution, we find 4.20 eV. Given that Wen et al. consider a cluster model, as opposed to our periodic stripe model, and given that there are small differences in the methodology of the calculations, there is overall good agreement. The exothermic substitutions found by Wen et al. can be directly explained by the different choices for carbon and sulfur references. For the situation considered in this work, we consider DMDS and DMS to be the relevant references for carbon and H_2S–H_2 to be the relevant references for sulfur, as these are the molecules that supply carbon and sulfur in the experiments.

4. Conclusion

From an interplay of STM, XPS, and DFT, we have thoroughly studied the energetics of incorporating carbon into MoS_2 nanoclusters when these are synthesized with the organosulfur agents such as DMDS or DMS. DMDS has a very high sulfidation potential, and from the STM studies, we find that the synthesized MoS_2 clusters are identical to those formed with H_2S, i.e., triangular, single-layered MoS_2 nanoclusters with the characteristic electronic brim edge state. Neither the STM nor the XPS results reveal any sign of carbon present at the edges or inside the MoS_2 nanoclusters. On the contrary, when the clusters are synthesized with DMS instead, we find that carbon is present on the surface of the nanoclusters before they are fully sulfided. The XPS binding energies for the carbon species on the surface are not consistent with the formation of a molybdenum carbide phase, and the carbon on the surface is found to desorb from the nanoclusters when these are annealed to higher temperature where crystalline, triangular MoS_2 nanoclusters are formed. Thus, the STM experiments do not indicate the presence of any carbidic-type carbon in MoS_2 nanoclusters. DFT calculations allow us to gain further detailed insight into the thermodynamic stability of carbon incorporation into MoS_2-based HDS catalysts under hydrotreating conditions. We found that substitution of sulfur by C, CH, or CH_2 is thermodynamically unfavorable for all relevant edge structures for the Mo-edge and the S-edge, if carbon is supplied by DMS or DMDS. This finding is in excellent agreement with the STM and XPS exper-

iments on the model catalysts, which revealed that the thermodynamically stable phase of the MoS_2 nanoclusters contains no carbon. A very important finding from the DFT calculations concerns the influence of the HDS environment. Under HDS conditions, the MoS_2 cluster edges expose less sulfur than under the sulfur-rich STM and XPS conditions, and it is found that this makes the exchange of sulfur with carbon even more unfavorable. The apparent lack of carbon in the STM and XPS experiments thus seems to suggest that carbon substitution is also very difficult under real HDS conditions.

The DFT results furthermore show that carbon incorporated into MoS_2 nanoclusters will not be stable during operation toward replacement by sulfur and the production of CH_4. Thus, although we have not considered all possible systems and conditions, we have obtained no evidence at all for the existence of surface or bulk carbide phases in HDS catalysts. Rather, our results illustrate that substitution of sulfur with carbon in MoS_2 nanoparticles is very difficult and energetically very unfavorable. Our results show that the choice of sulfiding agent may affect the size and morphology of the resulting nanoclusters. To what extent this may explain the previously reported activity differences needs to be studied further.

Acknowledgments

The iNANO group gratefully acknowledges financial support from The Danish Research Councils, The Strategic Research Council (NABIIT project "Development of new metal-oxide and -sulfide catalysts"), the Carlsberg Foundation, the Lundbeck Foundation, and the Villum Kann Rasmussen Foundation. J.V.L. and F.B. both acknowledge generous financial support from the European Research Council (ERC).

References

[1] H. Topsøe, B.S. Clausen, R. Candia, C. Wivel, S. Morup, J. Catal. 68 (1981) 433–452.
[2] H. Topsøe, B.S. Clausen, F.E. Massoth, Hydrotreating Catalysis, Springer, Berlin, Heidelberg, 1996.
[3] J.V. Lauritsen, M. Nyberg, J.K. Nørskov, B.S. Clausen, H. Topsøe, E. Lægsgaard, F. Besenbacher, J. Catal. 224 (2004) 94–106.
[4] M.V. Bollinger, K.W. Jacobsen, J.K. Nørskov, Phys. Rev. B 67 (2003) 085410.
[5] H. Schweiger, P. Raybaud, G. Kresse, H. Toulhoat, J. Catal. 207 (2002) 76–87.
[6] P. Raybaud, Appl. Catal. A – Gen. 322 (2007) 76–91.
[7] B.M. Vogelaar, P. Steiner, A.D. van Langeveld, S. Eijsbouts, J.A. Moulijn, Appl. Catal. A – Gen. 251 (2003) 85–92.
[8] H. Hallie, Oil Gas J. 80 (1982) 69–74.
[9] R.P. Silvy, P. Grange, F. Delannay, B. Delmon, Appl. Catal. 46 (1989) 113–129.
[10] S. Texier, G. Berhault, G. Pérot, V. Harlé, F. Diehl, J. Catal. 223 (2004) 404–418.
[11] C. Glasson, C. Geantet, M. Lacroix, F. Labruyere, P. Dufresne, J. Catal. 212 (2002) 76–85.
[12] R.R. Chianelli, G. Berhault, Catal. Today 53 (1999) 357–366.
[13] G. Berhault, A. Mehta, A.C. Pavel, J.Z. Yang, L. Rendon, M.J. Yacaman, L.C. Araiza, A.D. Moller, R.R. Chianelli, J. Catal. 198 (2001) 9–19.
[14] R.R. Chianelli, G. Berhault, B. Torres, Catal. Today 147 (2009) 275–286.
[15] S.P. Kelty, G. Berhault, R.R. Chianelli, Appl. Catal. A – Gen. 322 (2007) 9–15.
[16] R.R. Chianelli, M.H. Siadati, M.P. De la Rosa, G. Berhault, J.P. Wilcoxon, R. Bearden, B.L. Abrams, Catal. Rev. 48 (2006) 1–41.
[17] R.R. Chianelli, M.P. De la Rosa, G. Meitzner, M. Siadati, G. Berhault, A. Mehta, J. Pople, S. Fuentes, G. Alonzo-Nunez, L.A. Polette, J. Synchrotron Radiat. 12 (2005) 129–134.
[18] R.R. Chianelli, Oil Gas Sci. Technol. 61 (2006) 503–513.
[19] E. Lægsgaard, F. Besenbacher, K. Mortensen, I. Stensgaard, J. Microsc. 152 (1988) 663–669.
[20] S. Helveg, J.V. Lauritsen, E. Lægsgaard, I. Stensgaard, J.K. Nørskov, B.S. Clausen, H. Topsøe, F. Besenbacher, Phys. Rev. Lett. 84 (2000) 951–954.
[21] A. Tuxen, J. Kibsgaard, H. Gøbel, E. Lægsgaard, H. Topsøe, J.V. Lauritsen, F. Besenbacher, ACS Nano 4 (2010) 4677–4682.
[22] J.V. Lauritsen, M.V. Bollinger, E. Lægsgaard, K.W. Jacobsen, J.K. Nørskov, B.S. Clausen, H. Topsøe, F. Besenbacher, J. Catal. 221 (2004) 510–522.
[23] J.V. Lauritsen, J. Kibsgaard, S. Helveg, H. Topsøe, B.S. Clausen, E. Lægsgaard, F. Besenbacher, Nat. Nanotechnol. 2 (2007) 53–58.
[24] D.L. Adams, J.N. Andersen, FitXPS 2.12. <http://www.sljus.lu.se/download.html>.
[25] M.V. Bollinger, J.V. Lauritsen, K.W. Jacobsen, J.K. Nørskov, S. Helveg, F. Besenbacher, Phys. Rev. Lett. 87 (2001) 196803.
[26] J.V. Lauritsen, J. Kibsgaard, G.H. Olesen, P.G. Moses, B. Hinnemann, S. Helveg, J.K. Nørskov, B.S. Clausen, H. Topsøe, E. Lægsgaard, F. Besenbacher, J. Catal. 249 (2007) 220–233.
[27] B. Hinnemann, P.G. Moses, J. Bonde, K.P. Jorgensen, J.H. Nielsen, S. Horch, I. Chorkendorff, J.K. Nørskov, J. Am. Chem. Soc. 127 (2005) 5308–5309.
[28] B. Hinnemann, J.K. Nørskov, Topics Catal. 37 (2006) 55–70.
[29] B. Hammer, L.B. Hansen, J.K. Nørskov, Phys. Rev. B 59 (1999) 7413–7421.
[30] S.R. Bahn, K.W. Jacobsen, Comput. Sci. Eng. 4 (2002) 56–66.
[31] H.J. Monkhorst, J.D. Pack, Phys. Rev. B. 13 (1976) 5188–5192.
[32] K. Laasonen, A. Pasquarello, R. Car, C. Lee, D. Vanderblit, Phys. Rev. B 47 (1993) 10142–10153.
[33] D. Vanderbilt, Phys. Rev. B. 41 (1990) 7892–7895.
[34] N. Troullier, J.L. Martins, Phys. Rev. B 43 (1991) 1993–2006.
[35] T. Böker, R. Severin, A. Müller, C. Janowitz, R. Manzke, D. Voss, P. Krüger, A. Mazur, J. Pollmann, Phys. Rev. B 64 (2001).
[36] X.D. Wen, Z. Cao, Y.W. Li, J.G. Wang, H.J. Jiao, J. Phys. Chem. B 110 (2006) 23860–23869.
[37] G. Berhault, M. Lacroix, M. Breysse, F. Maugé, J.-C. Lavalley, L. Qu, J. Catal. 170 (1997) 37–45.
[38] J.H. Nielsen, L. Bech, K. Nielsen, Y. Tison, K.P. Jorgensen, J.L. Bonde, S. Horch, T.F. Jaramillo, I. Chorkendorff, Surf. Sci. 603 (2009) 1182–1189.
[39] C.D. Wagner, W.M. Riggs, L.E. Davis, J.F. Moulder, G.E. Muilenberg, Handbook of X-Ray Photoelectron Spectroscopy, Perkin-Elmer Corp., Edina, Minn, 1979.
[40] R.M. Petoral, K. Uvdal, J. Electron Spectrosc. 128 (2003) 159–164.
[41] M.J. Ledoux, P.H. Cuong, J. Guille, H. Dunlop, J. Catal. 134 (1992) 383–398.
[42] L. Ding, Y. Zheng, Catal. Commun. 7 (2006) 1035–1041.
[43] S. Texier, G. Berhault, G. Perot, F. Diehl, Appl. Catal. A – Gen. 293 (2005) 105–119.
[44] F. Abild-Pedersen, J. Greeley, F. Studt, J. Rossmeisl, T.R. Munter, P.G. Moses, E. Skulason, T. Bligaard, J.K. Nørskov, Phys. Rev. Lett. 99 (2007) 016105.
[45] E.M. Fernandez, P.G. Moses, A. Toftelund, H.A. Hansen, J.I. Martinez, F. Abild-Pedersen, J. Kleis, B. Hinnemann, J. Rossmeisl, T. Bligaard, J.K. Nørskov, Angew. Chem. Int. Edit. 47 (2008) 4683–4686.